Supplementary information

Surface layer formation in the earliest stages of corrosion of steel in CO_2-saturated brine at 80°C, studied by *in situ* synchrotron X-ray methods

B. Ingham, W. Holmes-Hewett, M. Ko, N. M. Kirby, M. H. Sk, A. M. Abdullah, N. J. Laycock and D. E. Williams

1 Additional figures:

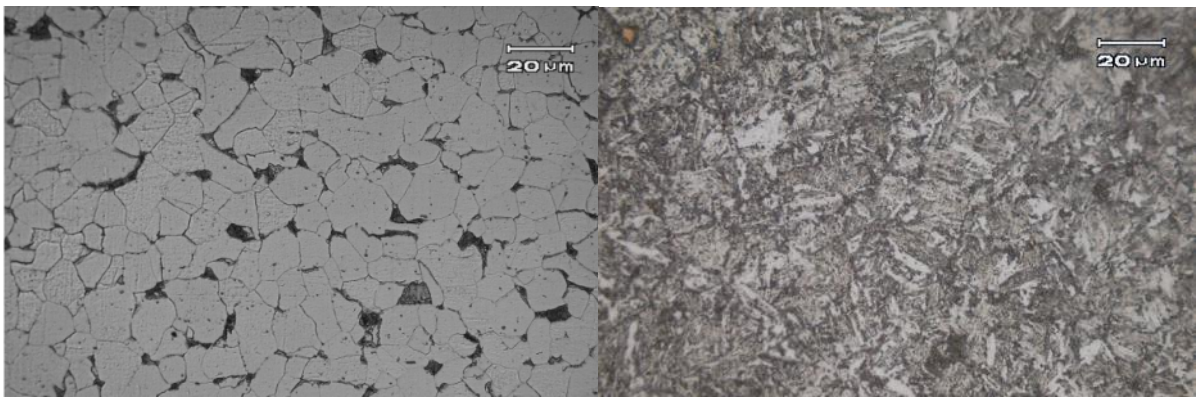

(a) (b)

Figure S1: Microstructure of the steels. (a) AISI 1006 mild steel; (b) API 5CT L80 1Cr0.25Mo pipeline steeel

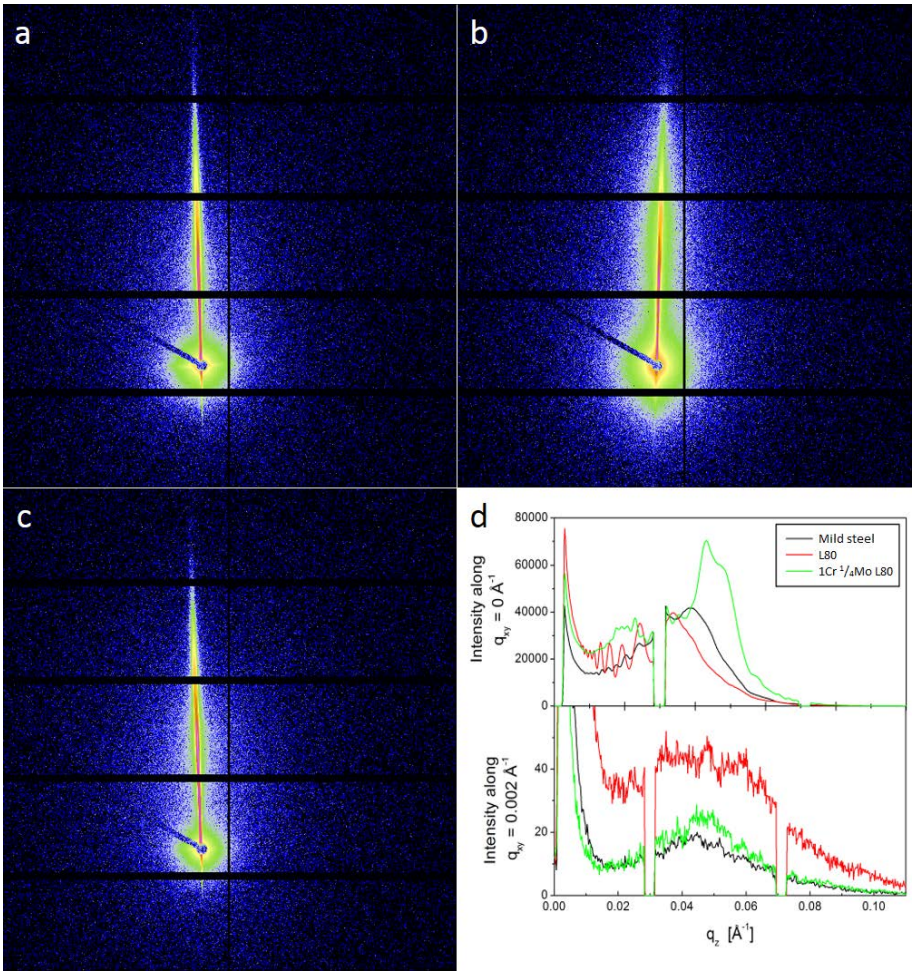

Figure S2. Experimental GISAXS images of as-prepared steel samples with no solution present: (a) mild steel, (b) L80, (c) 1Cr ¼Mo L80, (d) intensity versus q_z at q_{xy} = 0 Å^{-1} (specular) and q_{xy} = 0.002 Å^{-1} (off-axis) for each sample.

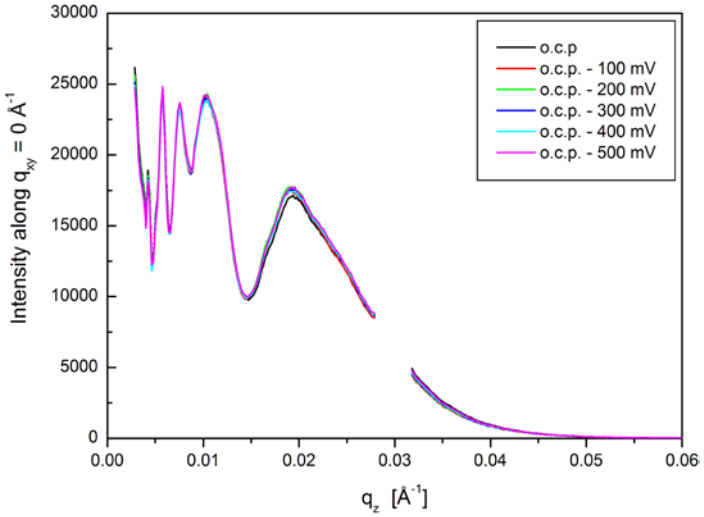

Figure S3. GISAXS specular scattering of an experiment where the mild steel electrode was negatively polarised to remove any air-formed surface film.

In each of the following figures, two cuts at constant q_{xy} for a selection of scans from each experiment is shown: the specular (on-axis) scattering at q_{xy} = 0 Å^{-1}, and the diffuse (off-axis) scattering at q_{xy} = 0.002 Å^{-1}. The small plots on the right of each figure show the same data, collated in time, with dotted lines illustrating how the main features observed are aligned.

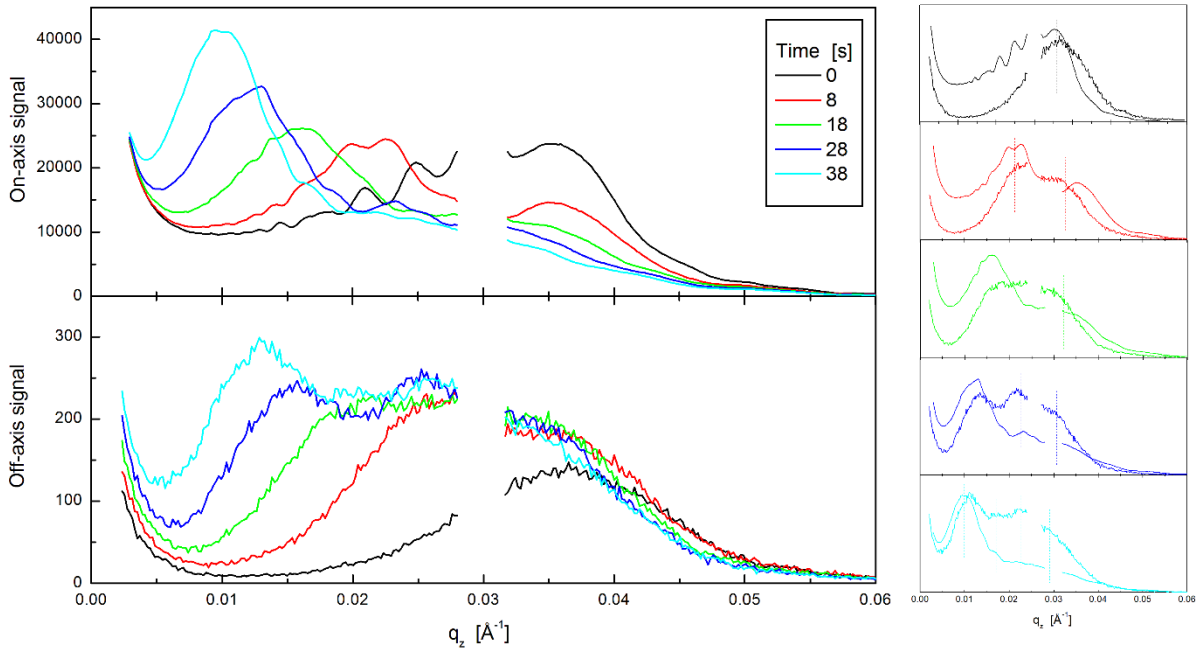

Figure S4 An experiment conducted on 1Cr ¼ Mo L80 steel at o.c.p. + 200 mV in a 0.5 M NaCl, CO_2-saturated solution with pH = 6.8 at 80°C.

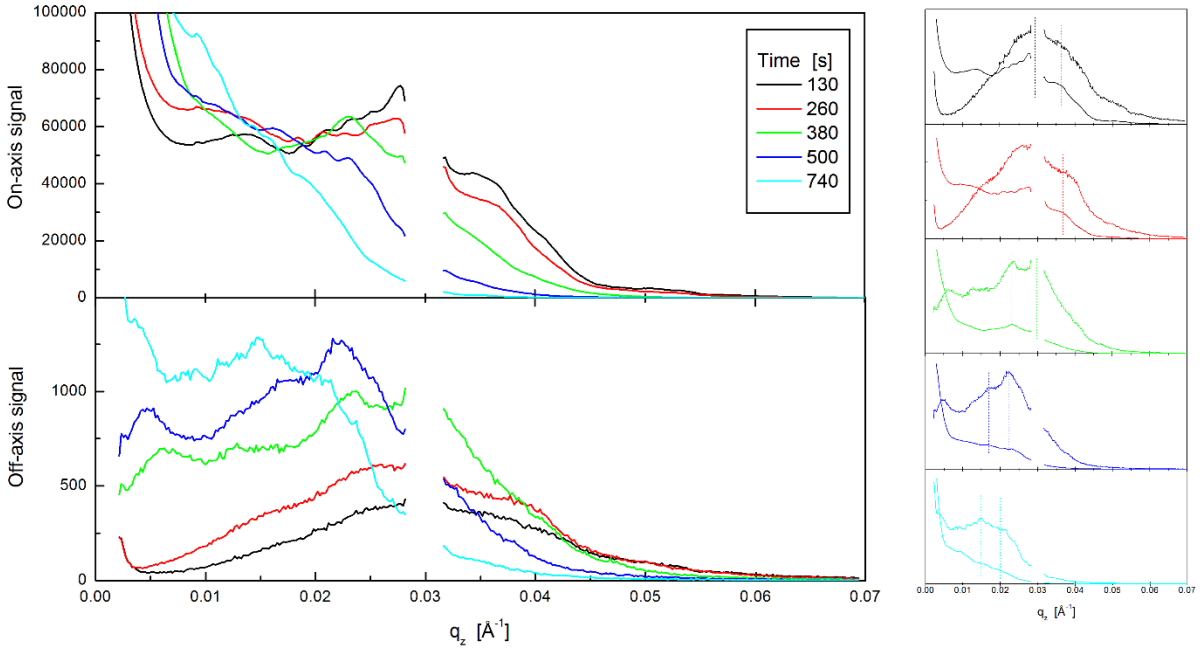

Figure S5. An experiment conducted on mild steel where the surface was electrochemically roughened by applying an anodic current (0.5 mA.cm^{-2} for 250 s, then increasing to 5 mA.cm^{-2}) in a 0.03 M HCl + 0.5 M NaCl electrolyte at room temperature.

2 Modelling of the origin of the oscillations on the specular peak

To understand the origin of the oscillations, we calculated some test patterns using the IsGISAXS program [1,2]. This uses the distorted wave Born approximation (DWBA) to calculate GISAXS patterns from objects on or buried in a substrate, with or without an overlayer present. We tested the hypothesis that they are due to the steel microstructure, namely the Fe_3C inclusions at the grain boundaries. The complex terms δ and β of the refractive indices are given in Table 1.

Table 1. Calculated complex index of refraction $n = 1 - \delta - i\beta$ for various species present in the steel system, at an X-ray energy of 15 keV. The critical angle $\alpha_c = \sqrt{2\delta}$.

Compound	Mass density [g.cm^{-3}]	δ	β
Fe	7.874	6.86×10^{-6}	2.92×10^{-7}
Fe_3C	7.694	6.73×10^{-6}	2.66×10^{-7}
$FeCO_3$	3.96	3.56×10^{-6}	7.27×10^{-8}
$Fe_2(OH)_2CO_3$	3.60	3.26×10^{-6}	7.40×10^{-8}
H_2O	1.0	1.026×10^{-6}	9.92×10^{-10}

The calculated scattering from these buried particles (Figure S6) exhibits form factor oscillations along the specular peak. These are similar to the experimental data.

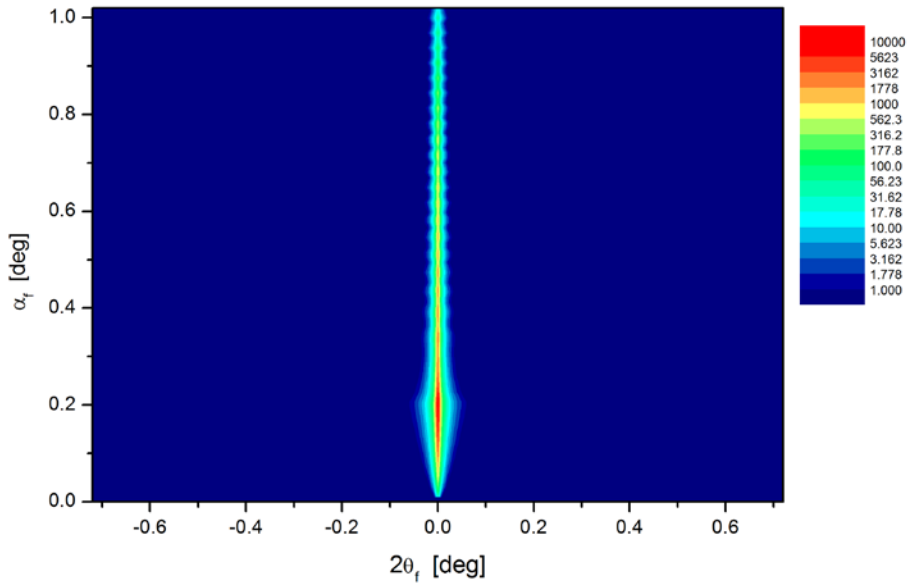

Figure S6. Theoretical GISAXS pattern for 300 nm Fe_3C grain boundary in Fe, calculated as 'buried particles' using IsGISAXS, at an incidence angle of 0.5°, X-ray energy 15 keV, polydispersity 0.3. Note the Yoneda peak at α_f = 0.2° and the intensity oscillations along the specular streak.

3 Computing the contribution to the scattering caused by the initial surface roughness

Another contributing factor to the broadness of the specular peak and the presence of diffuse scatter is the fact that although the electrode was polished to an optically smooth finish, the DWBA generally depends on the surface being atomically smooth. Roughness terms can be included as a perturbation [3], but only for small deviations, up to ~3 nm [4]. There are numerous methods for calculating diffuse scatter from rough surfaces [5-8], however to quickly test whether surface

roughness alone could account for the diffuse scatter observed, we used that of Ward [9], who gave simple equations in angular space for calculating the diffuse reflection of visible light. The radiance (reflected light) *L* is given by

$$L_r(\theta_r,\phi_r) = \int_0^{2\pi}\int_0^{\pi/2} L_i(\theta_i,\phi_i)\rho_{bd}(\theta_i,\phi_i;\theta_r,\phi_r)\cos\theta_i \sin\theta_i d\theta_i d\phi_i \qquad \text{[eq1]}$$

ρ_{bd} is the bidirectional reflectance distribution function (BRDF), θ is the polar angle (measured from the sample normal), ϕ is the azimuthal angle, and the subscripts *i* and *r* refer to incident and reflected components respectively.

For an isotropic surface with RMS roughness *R*, the BRDF is

$$\rho_{bd}(\theta_i,\phi_i;\theta_r,\phi_r) = \frac{\rho_d}{\pi} + \rho_s \frac{1}{\sqrt{\cos\theta_i \cos\theta_r}} \frac{\exp\left[-\tan^2\xi/R^2\right]}{4\pi R^2}$$

where ρ_d and ρ_s are the diffuse and specular reflectance respectively, and ξ is the angle between the sample normal and the reflection vector (equivalent to ***Q***).

The above equations were implemented in a computer program, using a Gaussian distribution to describe the horizontal and vertical beam divergence for $L_i(\theta_i,\phi_i)$. The widths in θ and ϕ were taken to be equal to the beam divergence values (200 µrad horizontal, 50 µrad vertical [10]). Calculated images for roughness values *R* of 0.001 and 0.002 are shown in Figure S6.

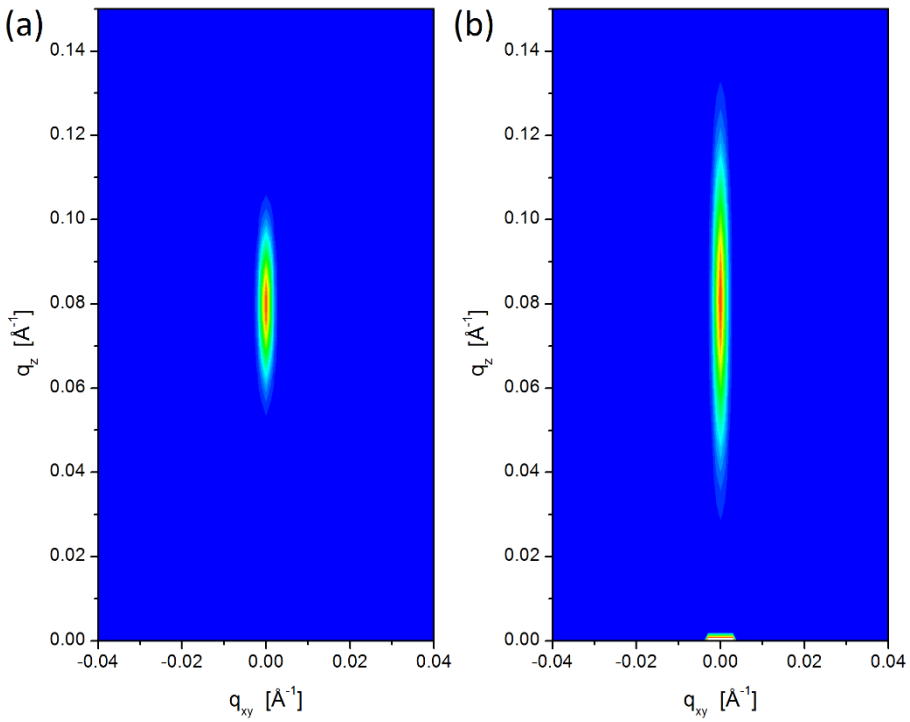

Figure S7. Calculated images of the diffuse scatter about the reflected beam for RMS roughness values of (a) *R* = 0.001 and (b) *R* = 0.002, according to equation 1.

The calculated images show a spot that is broader in the vertical direction than the horizontal. The extent of this broadening increases as the roughness increases.

4 Computation of the effect of surface roughness developing due to corrosion: Approximating the surface by a double sine function

The X-ray beam incident on the sample is divided into a large number of points, and the incidence angle at the point of intercept of each one is calculated. The reflected angle is then double this. A histogram is generated of the reflected angles.

The computational strategy is: Define the maximum x which a ray impinging on a flat surface at an angle α_i would intersect with some part of the surface (Figure S8). Define this as x_{max}.

Create an evenly spaced array of m values from zero to x_{max}. (Testing indicated that to obtain sufficient statistics, m should be at least 10 times the number of periods of the second level.)

Create an array of n values from zero to $\alpha_{f,\,max}$ for storing a histogram.

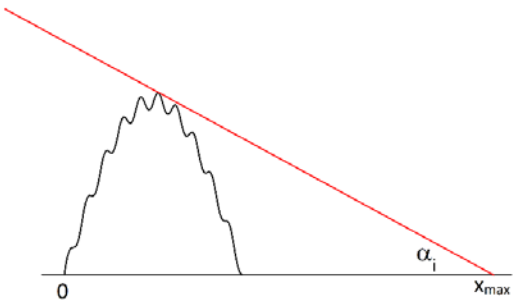

Figure S8. Schematic diagram showing how x_{max} is determined for the double sine function model.

For each x position, calculate the position where a ray striking the flat surface at an incident angle of α_i would intersect the surface. Calculate the gradient at this position and convert to an angle (η). The reflected angle, α_f, is equal to $\alpha_i + \eta$ (Figure S9). Increment the histogram division corresponding to α_f.

The vertical beam divergence can be included by applying a Gaussian distribution to α_f and adding to the relevant histogram divisions.

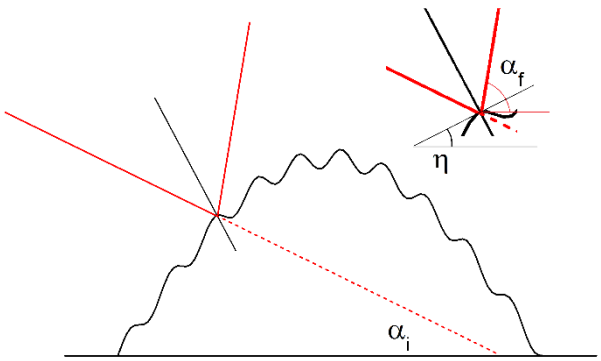

Figure S9. Schematic diagram showing key angles (α_i, α_f, η) in the double sine function model.

Results are shown in Figure S10 for various cases, each with the incidence beam split into 50,000 points.

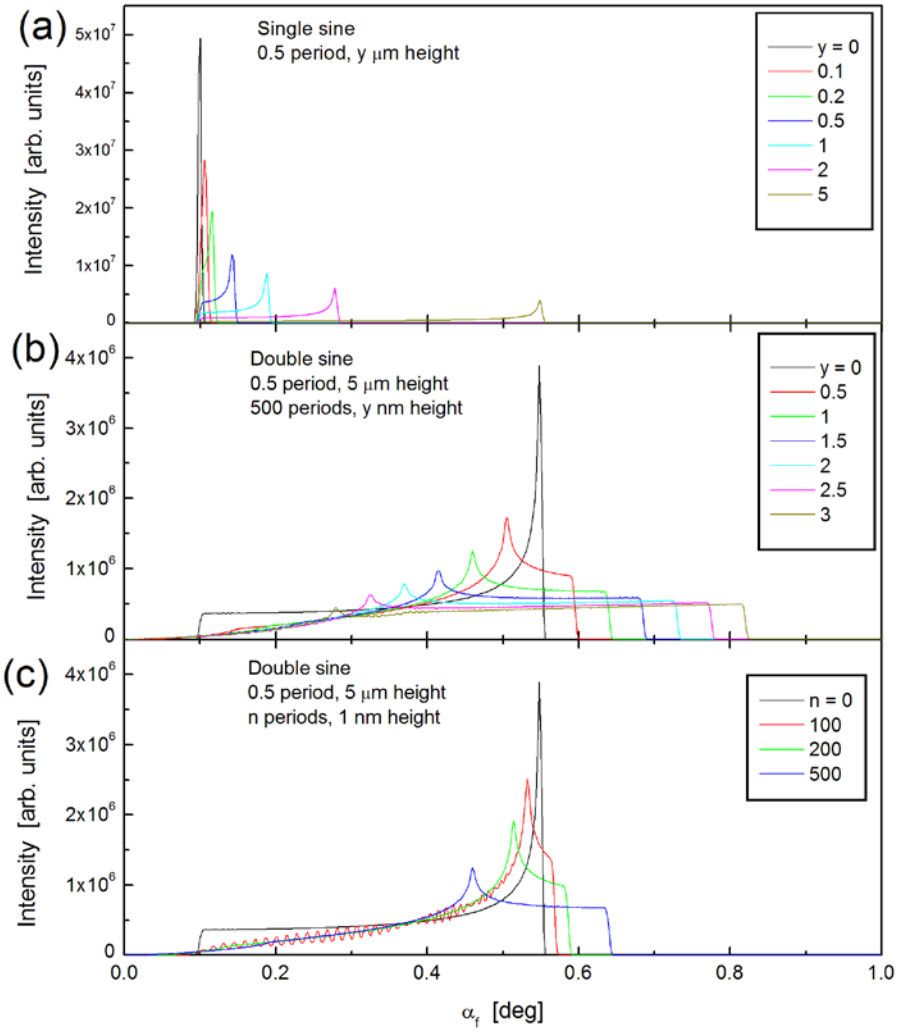

Figure S10. Calculated specular intensities for X-rays with incidence angle α_i = 0.1° scattering from an electrode surface approximated by a double sine function, showing the effect of increasing (a) height of primary sine function, (b) height of secondary sine function, (c) frequency of secondary sine function.

The effects of increasing curvature are to create a 'tail' extending from $\alpha_f = \alpha_i$ to the peak, which moves to higher angle as the curvature (i.e. height parameter) increases, while the intensity of the peak decreases. The macroscale curvature of the sample due to polishing is not expected to change significantly during the experiment:

The quantitative shift in peak position is related to the change in gradient. As shown in Figure S8, η = atan(g) where g denotes the surface gradient. Since α is fixed, we conclude that $\Delta\alpha_f = \Delta\eta = \Delta(\text{atan}(g)) \approx \Delta g$ for small values of g. Therefore, Δg can be obtained from the experimental data (i.e. $\Delta\alpha_f$ in radians) and used as a proxy measure to follow the development of surface roughness,

providing the initial maximum is at sufficiently high q_z to be resolved from the intense scattering around the direct beam.

References [i]

[i] [1] Lazzari, R. (2015). IsGISAXS http://www.insp.jussieu.fr/oxydes/IsGISAXS/isgisaxs.htm

[2] Lazzari, R. (2002). J. Appl. Cryst. 35, 406-421.

[3] Sinha, S. K., Sirota, E. B., Garoff, S. & Stanley, H. B. (1988). Phys. Rev. B 38, 2297-2311.

[4] Weber, W. & Lengeler, B. (1992). Phys. Rev. B 46, 7953-7956.

[5] Sinha, S. K. (1994). J. Phys. III France 4, 1543-1557.

[6] de Boer, D. K. G. (1994). Phys. Rev. B 49, 5817-5820.

[7] de Boer, D. K. G. (1995). Phys. Rev. B 51, 5297-5305.

[8] Pynn, R. (1992). Phys. Rev. B 45, 602-612.

[9] Ward, G. J. (1992). Computer Graphics 26, 265-272

[10] Australian Synchrotron (2016). "Beam divergence at sample position 140-260 µrad horizontal; 30 - 60 µrad vertical depending on focal position." http://synchrotron.org.au/aussyncbeamlines/saxswaxs/saxs-specifications